Impacts of drops of water and polymeric fluids on small targets

A. Rozhkov[†], B. Prunet-Foch, M. Vignes-Adler

LPMDI, UMR8108 du CNRS, University of Marne-la-Vallée, Bât. Lavoisier - 5, bd. Descartes, F-77454 Marne-la-Vallée Cedex 2, France

We have used small targets to investigate the drop impact process. This configuration has allowed us to better analyze the hydrodynamic effects, which are usually screened by the viscous liquid/substrate friction when impact occurs on a large plate. An obvious application is given by the spray of pesticides on ears of wheat or corn, and on any plants with spikes. Ink jet printing on a very rough substrate provides another example. It can also be seen as a model for drop impact on a hydrophobic plate when the effect of the viscous friction is negligibly small. The impacts of drops (d_i ~ 2.4–4.16 mm, v_i ~ 3.5–3.9 m/s) of water and of polymer solutions on a stainless steel disk (∅=3.7–7 mm) were therefore monitored by means of a high-speed photography technique. Upon collision of the drop with the target, the liquid was ejected in the shape of a circular flat (or conical) free lamella bounded by a rim from which liquid fingers and/or droplets detached. The lamella exhibited an apparent maximum diameter before it retracted and then collapsed. In-situ measurements of dynamical flow characteristics could be performed by generating Mach-type hydrodynamic instabilities in the lamella by means of a small obstacle placed close to the target. Main results are as follows. The duration of the effective liquid ejection was $3\times t_*$, where $t_*=d_i/v_i$ is the impact time scale. The rim formation was assigned to the unbalance of the capillary forces at the film periphery: this generated an external Taylor rupture wave propagating inwards, sweeping the liquid into a thickening rim. At the end of the lamella life, most of the drop liquid was accumulated in the rim. A very simple theoretical modelling of the lamella flow could predict the rim diameter. The finger formation and drop detachment were related to the different inertia of the droplets and of the liquid bridges between them in the rim, which in its turn was subjected to a high deceleration due to the capillary forces. Their larger inertia allowed the droplets to go ahead of the rim and form fingers. Polyoxyethylene additives (MW=4,000,000 and c = 1–1000 ppm wt) drastically changed the finger dynamics. Due to the polymeric fluid elasticity, the liquid fingers did not disintegrate into secondary droplets, but they transformed into thinning filaments with an attached droplet. Depending on the liquid rheology and the impact conditions, the droplets detached or returned into the rim: a splash threshold criterion was constructed.

1. Introduction

When a drop impacts a small disk-like target it evolves into a circular liquid lamella bounded by a thicker liquid rim, which expands and then retracts (Fig. 1). When the landing surface is a planar solid surface, the impact is controlled by the liquid inertia, surface tension and viscosity. Similar impact on a small disk-like target is solely controlled by inertia and surface tension if the impact Reynolds and Weber numbers are high [1]. Therefore, the use of small targets significantly simplifies the process and makes easier the understanding of

[†]Permanent address: Institute for Problems in Mechanics of Russian Academy of Sciences, 101(1) Prospect Vernadskogo, Moscow 119526, Russia

the hydrodynamics particularities and details, which are usually hidden by the effects of the liquid/solid viscous friction. With a small target, the effect of the surface tension becomes unambiguous; its effect on the rim dynamics is the same as in the case of impact on an extremely hydrophobic surface with contact angle equal to 180°. In addition, the comparison between the results obtained with the two kinds of impacts can enlighten the role of the viscous friction in the impact process.

The purpose of the present work is the understanding of the mechanisms that drive the lamella dynamics as well as its disintegration.

2. Experimental

Water and aqueous solutions of polyethylene oxide (PEO) with molecular mass M=4,000,000 and at concentrations c=1, 10, 100, 1000 wt ppm were used as drop liquids. The upper circular ends of stainless steel cylinders were used as targets. Drops were formed by means of dripping from the tip of a needle. The impacting drop diameters d_i ~ 2.4–4.16 mm were controlled by changing the needle diameter. The target diameters were d_t ~ 3.7–7.0 mm, the ratios d_t/d_i being kept close to 1.5. The drop impact velocities were v_i ~ 3.4-3.9 m/s. The process was visualized by means of high-speed video techniques.

Typical impacts of drops of water and of a PEO solution at c=100 wt ppm are displayed in Fig. 1. The lamellas resulting from the outwards ejection of the drop liquid are flat, and in both cases they approximately reach the same maximum diameter d_m that exceeds the target diameter d_t in about 4 times; they are also retracting at approximately the same rate [2]. We did not observe the retardation of the retraction phase reported before for the same polymeric solution in the case of impact on a planar surface [3].

3. Flow structure

During the radial ejection of the drop liquid from the target in the form of a liquid sheet, all the geometrical scales above the target in the flowing liquid are in the order of the impacting drop diameter d_i, and the velocity ones in the order of the impact velocity v_i. Therefore, the viscosity influence is negligible since the corresponding Reynolds number $Re=\rho v_i d_i/\mu \sim 10^4$ is high enough.

It is possible to imagine that the liquid is not supplied by the drop but by an equivalent point source with known time dependencies of the ejection velocity $v_s(t_s)$ and flow rate $q_s(t_s)$. The corresponding dimensionless functions $V_s(\tau_s)$, $Q_s(\tau_s)$ (where $V_s= v_s/v_i$, $\tau_s= t_s\, v_i/d_i$, $Q_s= q_s/(\, v_i \pi d_i^2/6)$) are *universal*, i.e. they are the same for any impacting drop if the impact Reynolds and Weber numbers are high enough [1]. Then, the flow on the target and in its close vicinity is exclusively defined by inertia and does not depend on other factors.

Once ejected, a liquid element is moving in the lamella with constant velocity. The flow in the lamella issued from the equivalent point source is axisymmetrical: the quantities $V_s(\tau_s)$, $Q_s(\tau_s)$ define the local velocity v and flow rate q in the lamella at point r and time t as [1]

$$V(\tau,Y)=V_s(\tau_s), \quad Q(\tau,Y)=Q_s(\tau_s)/(1+Yd/d\tau_s(1/V_s(\tau_s))), \quad Y=V_s(\tau_s)(\tau-\tau_s), \qquad (1)$$

Image number	Water	PEO, c=100 wt ppm
1	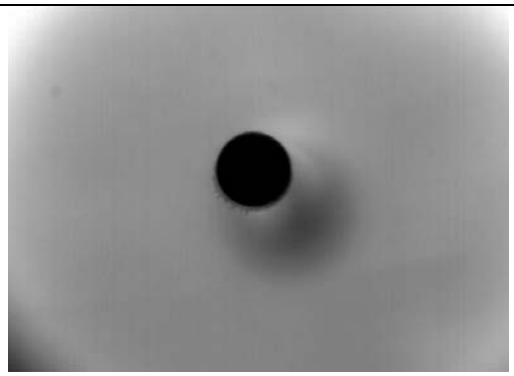	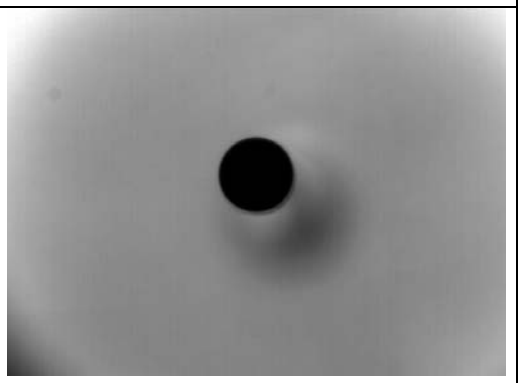
3	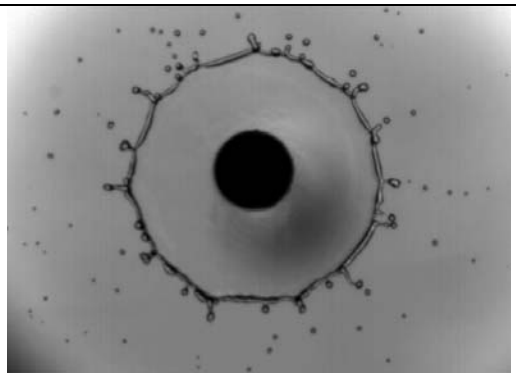	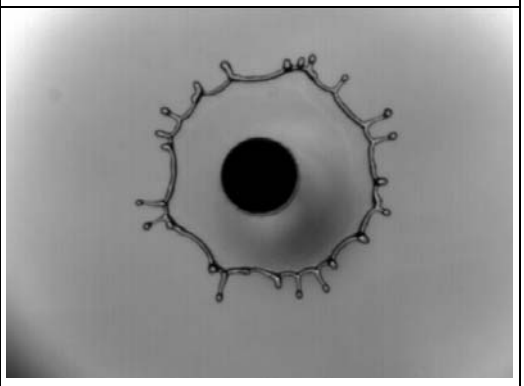
5	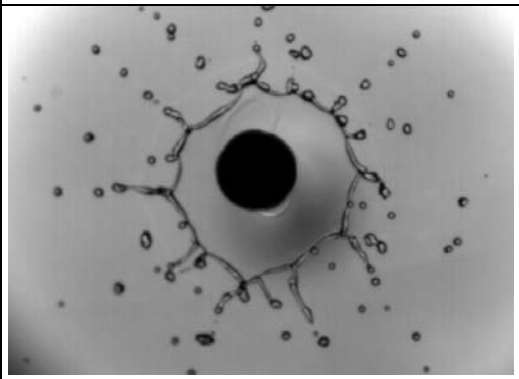	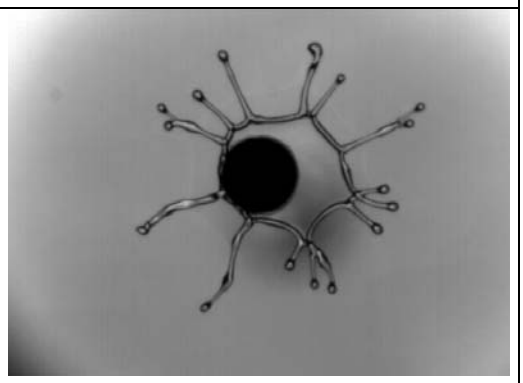
8	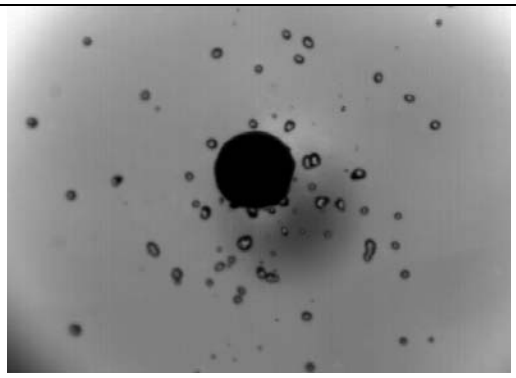	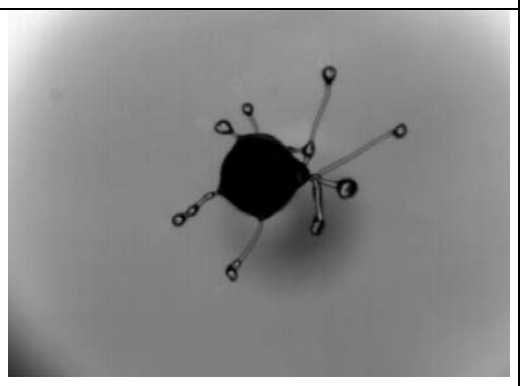

Fig. 1: Top views of free lamella resulting from the impact of a water drop (col. 2) and of a PEO solution drop (col. 3) on a disk-like target (black spot at the centre of the images, d_t=4.0 mm). d_i=2.7 mm v_i=3.87 m/s. The video recording rate is 1000 images per second.

where $V \equiv v/v_i$, $Q \equiv q/(v_i \pi d_i^2/6)$, r is the radial coordinate, $Y = r/d_i$, $\tau = tv_i/d_i$. The local flow rate q at point r is defined as the liquid volume, which flows through the contour of radius r per unit of time.

The functions $V_s(\tau_s)$, $Q_s(\tau_s)$ can be restored by a factor analysis as soon as some information about the flow inside the lamella is available. In particular we can get information by cutting the lamella with an external needle-like obstacle inserted in the lamella (Fig. 2). It generates two Mach-like rupture waves with an angle between them equal to 2φ, the value of which is directly related to the local flow parameters at the 'cutting' point $Y = Y_{ob}$ as [4]

$$(\sin\varphi)^{-2} = (We_i/24) VQ/Y_{ob}, \tag{2}$$

where $We_i = \rho v_i^2 d_i/\gamma$ is the impact Weber number, γ is the liquid surface tension.

We have shown in [1] that (i) about 2/3 of the drop volume has been ejected from the target at $\tau \sim 3$, (ii) the ejection velocity is a decreasing function of time and the ejection flow rate is approximately constant, (iii) as $\tau > 3$, the ejection becomes weak. Therefore, as a first approximation we can assume that

$$V_s = V_0/(1+B\tau_s), \quad Q_s = Q_0, \quad \tau_s \in [0,3] \tag{3}$$

where the unknown constants V_0, B, Q_0 are to be determined. Upon substitution in (1) and (2), we obtain the following relation between V_0, B, Q_0 and the value of $\sin\varphi$ measured at the obstacle:

$$1/(V_0 Q_0) + B\tau/(V_0 Q_0) = (\sin\varphi)^2 \, We_i/(24 Y_{ob}) \tag{4}$$

Measurements of $\sin\varphi$ in different points of the lamella, Y_{ob}, and at different times τ (Fig. 3) allow to validate the model (3). Best fit of the 166 experimental points with the relationship (4) determines the values of the flow parameter as $V_0 = 1.98$, $B = 0.94$, $Q_0 = 0.22$. In the framework of the proposed model, these values are the same for any drop impacting a small target at high Reynolds and Weber numbers.

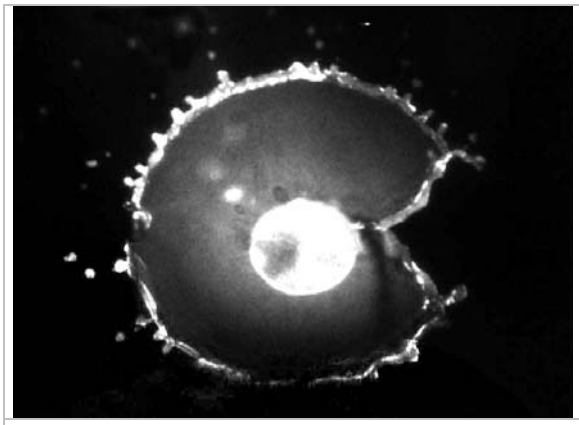

Fig. 2: Generation of a Mach-type rupture wave in the water lamella by means of a needle placed at the right side of the target. Image corresponds to the drop seen 1.85 ms after impact.

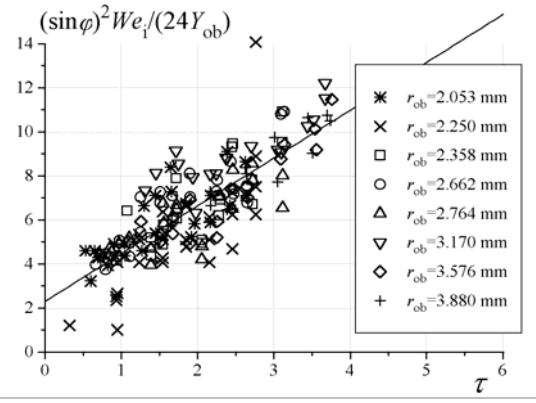

Fig. 3: Dependence of the combination $F = (\sin\varphi)^2 We_i/(24Y_{ob})$ as a function of the dimensionless time τ at different distances r_{ob} between the cutting obstacle and the centre of the target. Analysis shows that the data can be fitted by the linear function in Eq. (4) as $F(\tau) = 2.299 + 2.170 \cdot \tau$ (straight solid line).

Once the flow parameters are known, all the flow variables in the lamella can be obtained from (1). The distributions of the dimensionless velocity $V=v/v_i$ and of the dimensionless thickness $H=h/d_i$ in the lamella are reported in Fig. 4. To calculate the thickness, we have used the mass balance equation $q=2\pi rhv$. The liquid elements are moving in the lamella along the characteristic lines $dY/d\tau=V$ (Fig. 4) until they meet the rim (Fig. 5). The thickness of the moving elements, H, is decreasing in time as shown in Fig. 4.

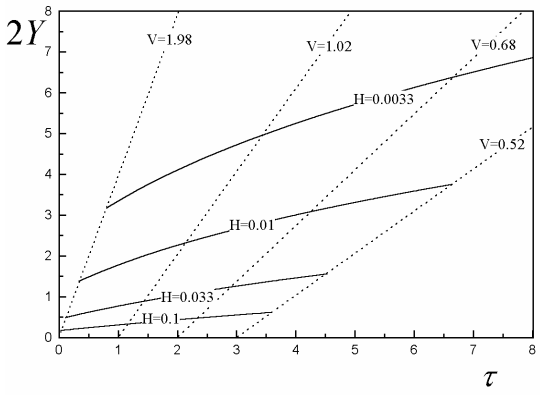

Fig. 4: Distribution of the velocity V and thickness H in the lamella for the liquid element that was ejected during the time interval [0,3].

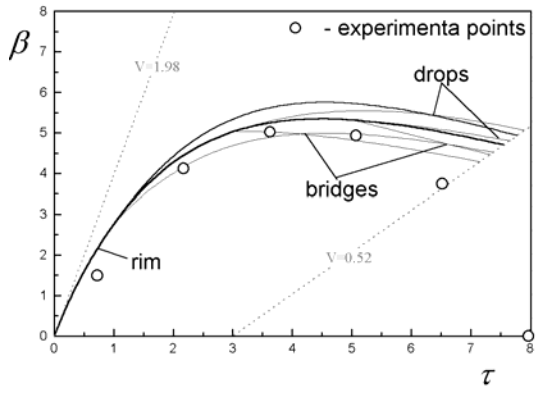

Fig. 5: The dependences of the lamella spread factor $\beta\equiv 2r_l/d_i$ as a function of dimensionless time τ. Circles are experimental points for the water lamella presented in Fig. 1. The curve 'rim' is the numerical solution of Eq. (5) for the same experimental conditions. The curves denoted 'bridges' and 'drops' show the rim fingering in the case of rim disintegration into thin and thick parts (Fig. 7).

4. Rim dynamics

The liquid rim is a rupture wave, which propagates against the stream under the action of surface tension consuming the lamella liquid [4]. If the rim is uniform, its dynamics is described by the equation of motion [1]

$$d/dt(mr_l(dr_l/dt))+\rho vhr_l(dr_l/dt-v)=-2\gamma r_l, \qquad (5)$$

where $m=M/(2\pi r_l)$ is the specific rim mass, M, the rim mass, r_l, the rim radial coordinate. The dependence $r_l=r_l(t)$ can be obtained by the numerical integration of Eq. (5) in the framework of the proposed model for the flow. The comparison between the theoretical and experimental results is given in Fig. 5. In Fig. 6, the maximum lamella spread factor $\beta_m\equiv 2r_{lm}/d_i$ (r_{lm} is the maximum lamella radius) and the dimensionless time τ_m at which the lamella diameter is maximum is plotted as a function of We_i. The available experimental data are also reported: present data and data from [1] were obtained for drop impact on small targets, whereas the other reported experimental data were obtained for drop impacting planar surfaces. The largest discrepancy between the theory and the experiment is observed for small β_m when the rim thickness is large compared to the lamella radius, whereas the theory considers the rim as having a zero thickness.

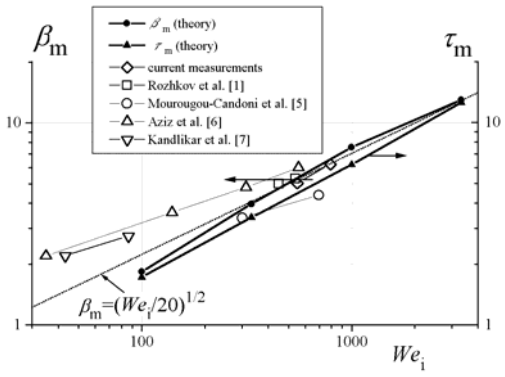

Fig. 6: Maximum lamella spread factor β_m and dimensionless time τ_m at which β is maximum as a function of the impact Weber number We_i.

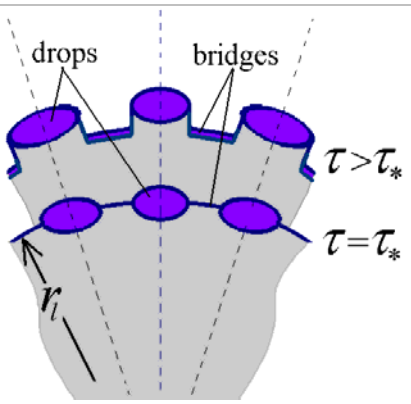

Fig. 7: Due to higher inertia, drops in the rim are less delayed than bridges under the action of the surface tension.

The developed theory can also be applied to drop impacts upon planar surfaces if the viscosity influence is negligible. An estimation of the thickness of the viscous boundary layer in the spreading drop shows that it takes place if $(\beta_m/8)^{1/2}We_i/Re_i^{1/2} \ll 1$. The presentation of the data on the impact on plane surface was made with a modified Weber number $We_{is}=We_i/((1-\cos\theta_a)/2)$, where θ_a is the dynamic advancing contact angle to take into account the influence of the liquid/solid surface interaction.

The results in Fig. 6 show that $\beta_m(We_i)$ as well as $\tau_m(We_i)$ can be approximated by the relations $\beta_m \sim \tau_m \sim (We_i/20)^{1/2}$. Hence, the time at which the lamella maximum diameter is reached, t_m, is given by the formula $t_m \sim \rho^{1/2} d_i^{3/2}/(20\gamma)^{1/2}$. It does not depend on the impact velocity and it is varying with the impacting drop diameter as $d_i^{3/2}$. The latter result indicates that the lamella lifetime (which is of order $O(t_m)$) is varying in a similar manner. This result compares well with the experimental observations by Richard et al. [8].

5. Fingering

Suppressing most of the substrate influence has allowed us to better understand the fingering and splashing mechanisms (Fig. 1). Two factors are dominating: first, the liquid rim is subjected to capillary instability and it is getting thick parts –the drops– and thin parts –the bridges between the drops–, secondly, all the liquid elements of the rim are subjected to a high deceleration under the action of the surface tension during the lamella growth and retraction. Under these circumstances, the more massive drops are decelerating less than the lighter bridges (Fig. 7). The drops overtake the bridges, which generates the fingering pattern and the subsequent splashing.

To model this process, we have assumed that the previously uniform rim was disintegrated into drops and bridges at time $\tau=\tau_*$. The drop and the bridge motion equation is again Eq. 5. It is equivalent to say that at τ_* the specific rim mass m in Eq. 5 increases in two times for the parts of the rim that include drops, and becomes zero for the part of the rim, which includes bridge. The following trajectories of the drops and bridges can therefore be obtained from the numerical integration of Eq. 5. The solutions are presented for $\tau_*=1$, 3 and 5 in Fig. 5. The difference between the trajectories of the drops and the ones of the bridges is significant, which provokes the detachment of the drops from the rim and generates splashes.

6. Impacts of polymeric drops. Splash threshold criterion

As can be observed in Fig. 1, col 3, in the case of drop impact of a polymeric solution, the secondary droplets, which previously detached from the rim, are now pulled back towards the target by means of forming thin filaments. The figures 8 and 9 show the lamella disintegrations of the less concentrated polymeric solutions.

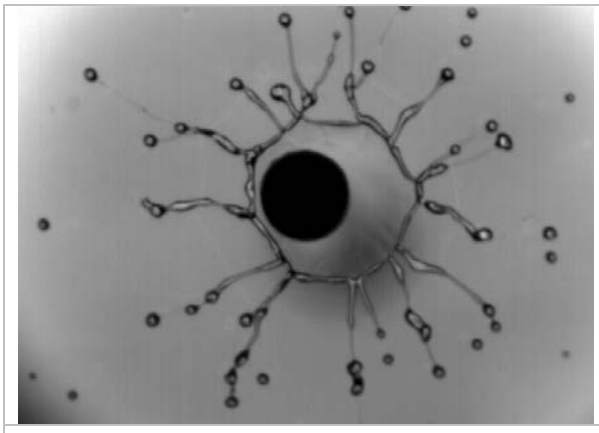

Fig. 8. Drop of PEO solution at c=1 wt ppm seen 6 ms after impact.

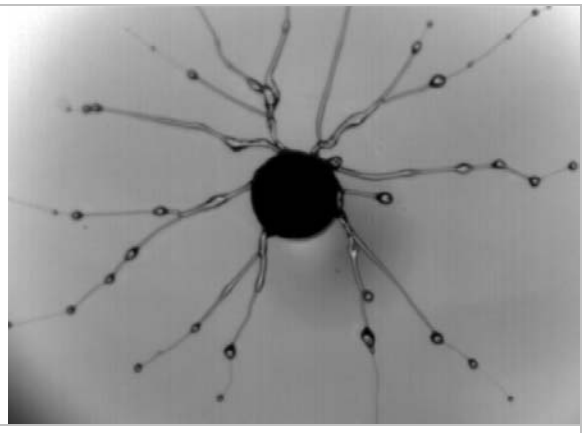

Fig. 9. Drop of PEO solution at c=10 wt ppm seen 6 ms after impact.

The filaments of the more dilute solutions look thinner and they do not drive back the secondary droplets as efficiently as the filaments of the most concentrated PEO, c=100 wt ppm do. Figure 8 clearly displays that the filaments break up before the secondary droplets reach back the main drop. From this simple observation, one can conclude that splashing happens if the filament lifetime is shorter than the time necessary for the droplet to reach the main drop.

Theoretical and experimental studies showed that the filament lifetime is in the order of 3θ [9]; during this time the filament is thinning as $a=a_0\exp(-t/(3\theta))$ [10], and the axial force in the filament is equal $f=\pi a\gamma$ [11], where θ is the liquid relaxation time, a is the filament diameter, a_0 is the initial filament diameter. One can show that the motion equation of the retracting secondary droplet under the action of the filament axial elastic force is $mdr^2/dt^2=-f$, where r is the radial coordinate of the secondary droplet [2] The solution is

$$R(T) = R_m + 1 - \exp(-T) - T\,, \tag{6}$$

where $R(T)=r/(\pi a_0\gamma(3\theta)^2/m)$, $R_m=r_{lm}/(\pi a_0\gamma(3\theta)^2/m)$, $T=t/(3\theta)$.

The droplet detaches if the solution of Eq. (6), $R(T)$, is positive at T=1 (instant of the filament rupture), and it is reaching the main drop if $R(T)$ is negative at T=1. Which one of these case occurs, depends on the parameter R_m. Calculations gives the critical value R_m=2.05 for $R(1)$=0. Therefore, if R_m>2.05, there is splashing, if R_m<2.05 then the droplets reaches the main drop before the filament can rupture and the drop saves its continuity. Considering the capillary rim instability as of Rayleigh type, assuming that the polymer additives do not significantly influence the flow in the lamella (see, for example, Fig. 1), and using the above estimation, the splashing threshold criteria R_m=2.05 can be reformulated as

$$(\rho d_i^3/(\gamma\theta^2))\cdot We_i^{\chi}=K \tag{7}$$

where χ=3/8, K=1140. If the left hand side of Eq. (7) is larger than this value of K then splashing happens, if not, then the lamella does not disintegrate.

Measurements of the relaxation time of PEO solutions, c=1, 10 and 100 wt ppm with the Liquid Filament Rheometer [12] give the values θ =0.368, 1.79 and 8.0 ms. In these cases, the calculations (other parameters correspond to situations of Figs. 1, 8, and 9) give 20637, 872 and 44 for the values of the left hand side of Eq. (7). The case of the PEO solution c=10 wt ppm is the closest to the critical situation which is characterised by K=1140. Actually, the lamella of PEO solution c=10 wt ppm only lost a few droplets whereas the main drop mass was accumulated at the target. The lamella of PEO, c=1 wt ppm disintegrated into droplets (20637>K), the lamella of PEO, c=100 wt ppm saved the liquid continuity (44<K).

On the other hand, the relation (7) can be considered as an empirical formula, the parameters χ and K of which are evaluated from experimental observations.

7. Acknowledgment

A.R. is very grateful to the University of Marne-la-Vallée for providing him a professorship position during his stay at the LPMDI.

References

[1] Rozhkov A, Prunet-Foch B, and Vignes-Adler M 2002 *Phys. Fluids* **14** 3485-3504
[2] Rozhkov A, Prunet-Foch B and Vignes-Adler M 2003 *Phys. Fluids, in press*
[3] Bergeron V, Bonn D, Martin J-Y and Vovelle L 2002 *Nature* **405** 772-5
[4] Taylor G I 1959 *Proc. Roy. Soc. London* **A253** 313-21
[5] Mourougou-Candoni N, Prunet-Foch B Legay F and Vignes-Adler M 1999 *Langmuir* **15** 6563-74
[6] Aziz S D and Chandra S, 2000 *International Journal of Heat and Mass Transfer* **43** 2841-57
[7] Kandikar S G, Steinke M E and Singh A, 2001 *Proceedings of NHTC`01, 35th National Heat Transfer Conference, June 10-12, 2001, Anaheim, California*, #11672
[8] Richard D, Clanet C and Quéré D, 2002 *Nature* **417** 811
[9] Bazilevsky A V, Entov V M, Lerner M M and Rozhkov A N 1997 *Polymer Science* **A39**, 316-24
[10] Bazilevsky A V, Entov V M and Rozhkov A N 1990 *Proceedings of the Golden Jubilee Meeting of the British Society of Rheology and Third European Rheology Conference. Edinburgh, UK, 3–7 September 1990* 41-3
[11] Bazilevsky A, Rozhkov A and Stavitsky A 1994 *Proceedings of the Fourth European Rheology Conference, Sevilla, Spain, 4-9 September 1994*, 468-70
[12] Bazilevsky A V, Entov V M and Rozhkov A N 2001 *Polymer Science* **A43** 716-26